A Novel Metamaterial-Based Orthomode Transducer With Symmetric Port Parameters

Lingqi Kong, Yi Huang, *Fellow, IEEE*, and Alexander G. Schuchinsky, *Fellow, IEEE*

***Abstract*— This article presents a novel metamaterial-based orthomode transducer (Meta-OMT) with symmetric port parameters, surpassing those of conventional OMTs. Using the polarization modulation properties of metamaterials, this design achieves complete port symmetry, enabling all three ports to serve as input terminals for the OMT. By harnessing the high polarization selectivity of metamaterials, the isolation of cross-polarized signals is significantly enhanced. Within the operating frequency range of 9.4–10.6 GHz, this Meta-OMT achieves low insertion loss ranging from 0.1 to 0.5 dB and facilitates efficient signal transmission. Moreover, it exhibits exceptional isolation capabilities, with isolation levels exceeding 40 dB for both co-polarization and cross-polarization signals and reaching 50 dB in 80% of the operating frequency band.**

***Index Terms*— Asymmetric metasurface, metamaterial, orthomode transducer (OMT), polarization conversion.**

I. Introduction

ORTHOMODE transducers (OMTs) are the critical components in many telecommunication and radar systems. They are widely used for detecting, measuring, and tracking targets [1]. The antenna in a radar system is typically linearly polarized, meaning that the electric field vector has a fixed direction, and it can only receive signals polarized in that direction. However, in some applications, it is necessary to receive signals from different directions and polarizations. As a result, an OMT is needed to solve this problem, and it was first proposed by Tompkins [2]. An OMT is shown in Fig. 1. It can divide the two orthogonal polarization components of the incoming signal and transmit them to two separate output ports, where the signals are processed independently. Dividing the input signal into two orthogonal polarized signals using an OMT provides the following benefits [3], [4], [5].

1) *Signal Isolation:* The signals of the two orthogonal polarizations have low interference between them. When multiple signal sources are in a transmission or processing environment, dividing orthogonal polarizations of the signals reduces crosstalk and interference.
2) *Wideband Transmission:* Orthogonally polarized signals offer a broader effective bandwidth/capacity. By dividing a signal into two orthogonal polarizations, it is possible to transmit more information simultaneously and increase the capacity and rate of signal transmission.
3) *Antenna Design:* The use of orthogonally polarized signals can improve antenna performance. By tailoring the signal characteristics, antenna systems can be designed to have better performance, e.g., gain, directivity, and interference rejection capabilities.

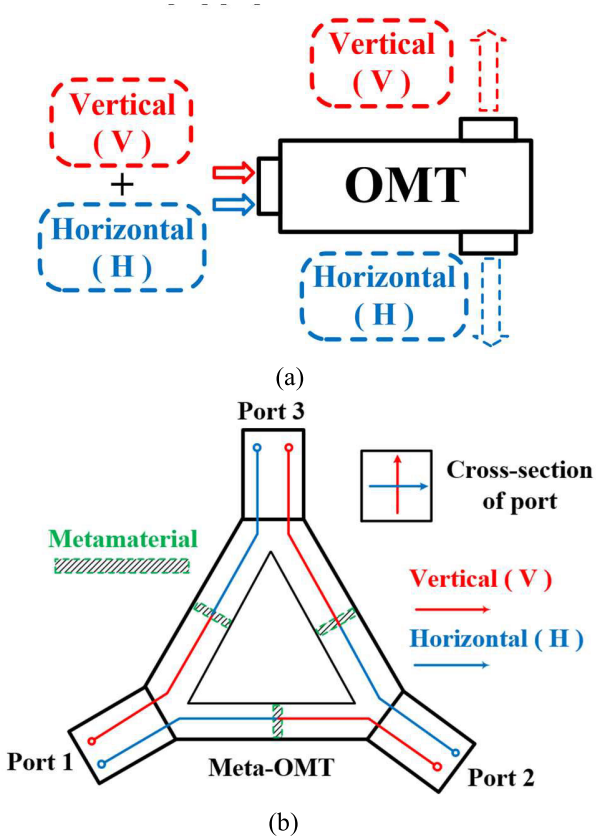

Fig. 1. Schematics of (a) conventional OMT and (b) Meta-OMT, where the solid lines show how the orthogonal signals flow in the structure and are converted by the metamaterials.

In recent years, OMTs have been extensively studied and developed. They can be divided into several groups based on the OMT design and functionality. OMTs can be realized as waveguide OMTs [1], [6], [7], [8], [9], [10] and planar OMTs [11], [12], [13], [14], [15], [16], [17].

Waveguide OMTs have the advantages of broad bandwidth and low losses but tend to have larger physical dimensions and

Manuscript received 30 June 2023; revised 16 September 2023; accepted 22 October 2023. *(Corresponding author: Yi Huang.)*

The authors are with the Department of Electrical Engineering and Electronics, University of Liverpool, L25 7YD Liverpool, U.K. (e-mail: lingqi.kong@liverpool.ac.uk; yi.huang@liverpool.ac.uk; a.schuchinsky@liverpool.ac.uk).

Color versions of one or more figures in this article are available at https://doi.org/10.1109/TMTT.2023.3329727.

Digital Object Identifier 10.1109/TMTT.2023.3329727

are relatively heavy as compared to planar OMTs. Compact size and ease of integration are the advantages of planar OMTs, but they have a lower power handling capability and higher losses.

The OMTs can also have symmetric and asymmetric designs for different application requirements and specific system designs. Symmetric OMTs [3], [7], [18], [19], [20] achieve a balanced power distribution and a precise polarization separation, commonly used in antenna systems, radar, and radio astronomy. Asymmetric OMTs [5], [21], [22], [23], on the other hand, introduce power imbalance and are employed in applications, where specific power distribution is required, e.g., in satellite communications.

Another type of OMT is called dual-mode OMT, which is designed to handle two different frequency bands simultaneously, allowing for the separation and combination of signals in each band [24], [25], [26].

The functionality and performance of OMT can be further enhanced with the use of metamaterials. Metamaterials are artificially engineered media that exhibit electromagnetic properties, which are not found in natural materials [27], [28]. The electromagnetic response of metamaterials arises from their structural design rather than their chemical composition. This allows them to manipulate the wave propagation in unconventional ways [29]. One of the most interesting research areas of metamaterials is polarization control, which can be associated with asymmetric transmissions or polarization conversion [30], [31], [32], [33], [34]. However, metamaterials are barely used in OMT designs so far to optimize the device's performance and expand its functionality.

In this article, a novel method for the design of OMTs using metamaterial polarization rotators is proposed and analyzed. As shown in Fig. 1, this metamaterial-based OMT (Meta-OMT) differs from conventional OMTs. Namely, in addition to the basic OMT function of separating orthomode signals, it makes all three ports usable as input ports with fully symmetrical port coefficients. This enhances its functionality and application versatility. In this article, the EM waves with vertical and horizontal electric fields are defined as vertically and horizontally polarized EM waves, respectively. The design utilizes the polarization separation capability of metamaterials, providing polarization isolation over 40 dB between co-polarization and cross-polarization in the Meta-OMT. The design details are presented in Section II and discussed separately in three parts. In Section III, the prototype of this design is fabricated and measured, verifying the feasibility and performance of Meta-OMT and demonstrating a good agreement with the simulations. In Section IV, brief conclusion and potential research directions of Meta-OMTs are discussed.

II. Meta-OMT Design

The intricate nature of the Meta-OMT structure necessitates a comprehensive explanation of its design. It is divided into three distinct components.

1) Y-shaped polarization separator.
2) Polarization conversion metamaterials in the waveguide.
3) Amalgamation of both to form the Meta-OMT.

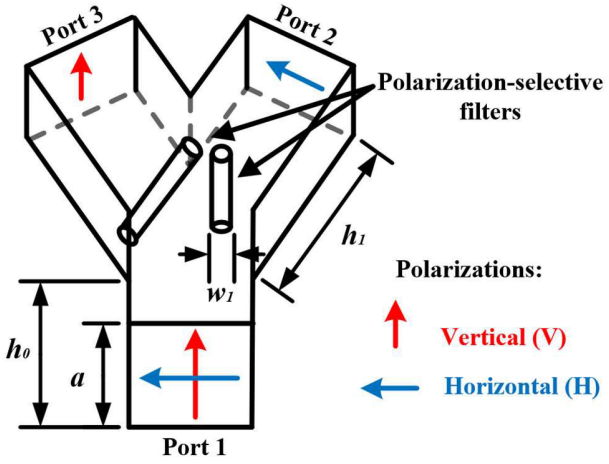

Fig. 2. Structure diagram of the Y-shaped polarization separator with dimensions: $\boldsymbol{a} = 18$ mm, $\boldsymbol{h_0} = 20.0$ mm, $\boldsymbol{h_1} = 50.0$ mm, and $\boldsymbol{w_1} = 1.5$ mm.

A. Y-Shaped Polarization Separator

The design of the Y-shaped polarization separator incorporates the overall functionality and meets the performance requirements of the Meta-OMT. Its functionalities primarily focus on the following aspects.

1) Polarization separation capability of the Y-junction.
2) Isolation between co-polarized and cross-polarized waves.
3) Symmetry of port parameters of the complete Meta-OMT.

These three features are elaborated as follows.

The structure of the Y-shaped polarization separator is based on a square waveguide with a side length of $\boldsymbol{a}$, as depicted in Fig. 2. Two matching metallic pins with radii of $\boldsymbol{w_1}$ are placed orthogonally at the inputs of waveguides, leading to ports 2 and 3. The pins serve the purpose of initial polarization separation and orthogonal mode matching. As shown in Fig. 2, horizontally polarized waves propagate only toward port 2 and are blocked from port 3, while vertically polarized waves exhibit the opposite behavior.

The transmission and reflection characteristics of the Y-shaped polarization separator are shown in Fig. 3(a). In the frequency band of 9–11 GHz, the insertion loss of vertically polarized wave is 0.8–1.0 dB between Ports 1 and 2, while the loss of the horizontally polarized waves between Ports 1 and 3 is 0.1–0.4 dB. The reflection coefficients for both polarizations exceed 10 dB.

Since the input signals are orthogonal dual-polarized waves, it is necessary to examine the co- and cross-polarization isolation between the ports. Co-polarization isolation is depicted in Fig. 3(b) in the frequency band of 9–11 GHz. All port pairs exhibit co-polarization isolation above 10 dB, except for slightly lower isolation between Ports 2 and 3 at vertical polarization. The isolation for horizontal polarization exceeds 15 dB. The cross-polarization isolation is shown in Fig. 3(c). As the design maintains the polarization structure and effectively utilizes the two metallic rods for polarization selection, the resulting cross-polarization isolation exceeds 60 dB, and these characteristics are further improved when a metamaterial is integrated into the Y-shaped polarization separator.

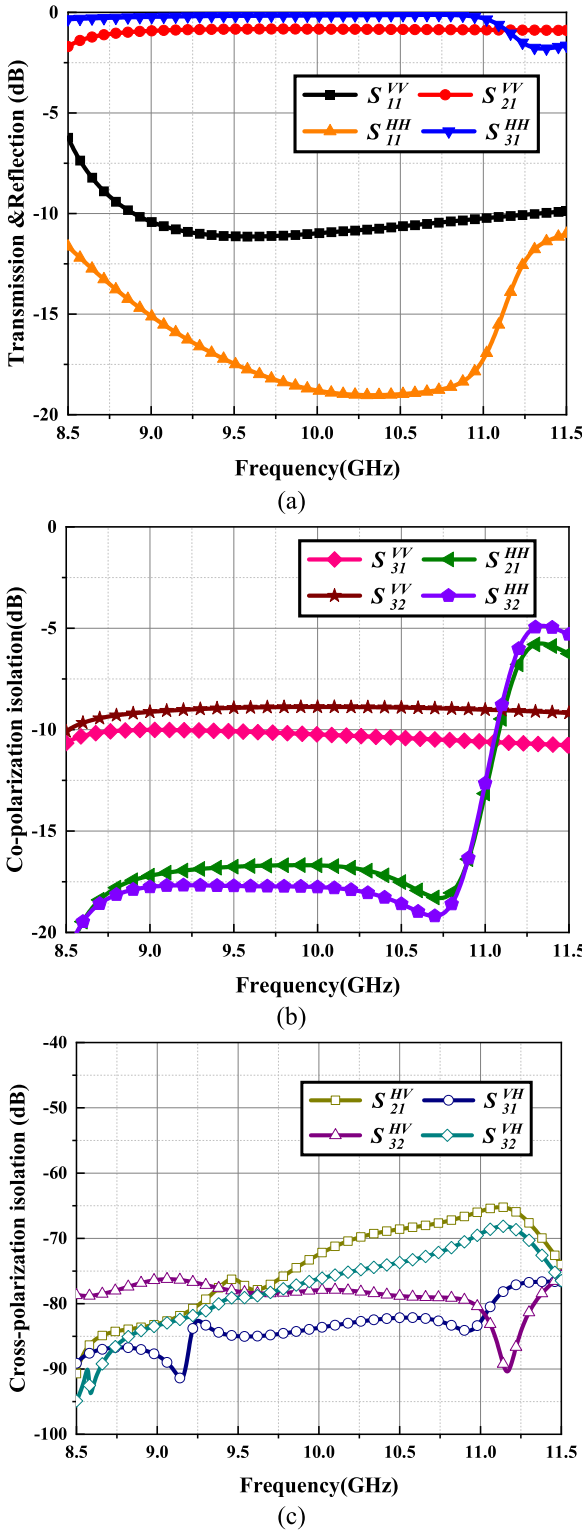

Fig. 3. S-parameters of the Y-shaped polarization separator. (a) Transmission and reflection coefficients. (b) Co-polarization isolation coefficients. (c) Cross-polarization isolation coefficients.

B. Metamaterials for Polarization Conversion

The metamaterial inclusion proposed for the polarization conversion is illustrated in Fig. 4. It is placed inside a metallic waveguide and is tightly connected to the metallic walls surrounding it. The upper and lower layers consist of metal polarization selectors with vertical and horizontal gaps.

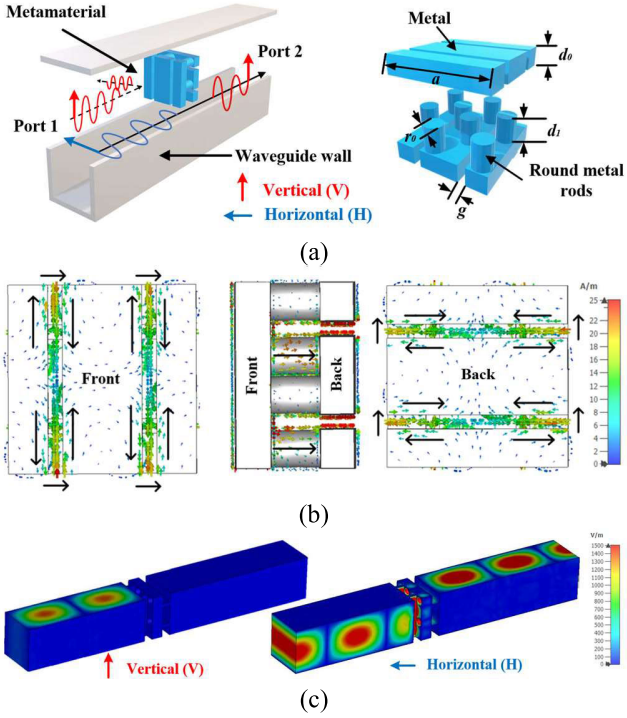

Fig. 4. (a) Configuration and dimensions of the metamaterial with polarization conversion within a waveguide. The metal bar length and thickness are $\boldsymbol{a} = 18$ mm and $\boldsymbol{d_0} = 3.4$ mm, and they are separated by the gap of width $\boldsymbol{g} = 1.4$ mm. The two layers of the orthogonal bars are connected by round metal rods with a diameter of $\boldsymbol{r_0} = 3.6$ mm and length $\boldsymbol{d_1} = 4.8$ mm. (b) Surface current distribution of metamaterial at 10 GHz. (c) E-field distribution for the input vertically and horizontally polarized waves at 10 GHz.

The metamaterial inserts primarily serve two functions.

1) Polarization rotation.
2) Polarization selection.

Namely, the proposed structure allows only a single specific polarization of electromagnetic field to pass through, while reflecting the other polarization. Such polarization rotation property is one typical function of chiral metamaterials [35]. Besides, the passing waves undergo polarization rotation with low insertion loss when transmitted to the output end. The details of the working principles of this metamaterial in the waveguide will be discussed in Section II-C.

As shown in Fig. 4(a), the first layer of the structure consists of a mesh-like arrangement that serves for polarization selection. Therefore, it only allows the wave with a horizontally polarized electric field to pass through and convert into a vertically polarized wave. The functions of polarization selection and rotation are illustrated by the E-field distribution pattern in Fig. 4(c).

A surface current distribution at the center frequency of 10 GHz has been given in Fig. 4(b). The in-phase currents on the two short sides of the slots can be seen on the front layer of the metamaterial, while the out-of-phase currents along the long edges cancel out. The slots on the top layer and waveguide walls act as a resonator at 10 GHz. The resonator receives the signal from the forward EM wave and converts it into the surface current at the back of the structure, rotating polarization of the EM wave.

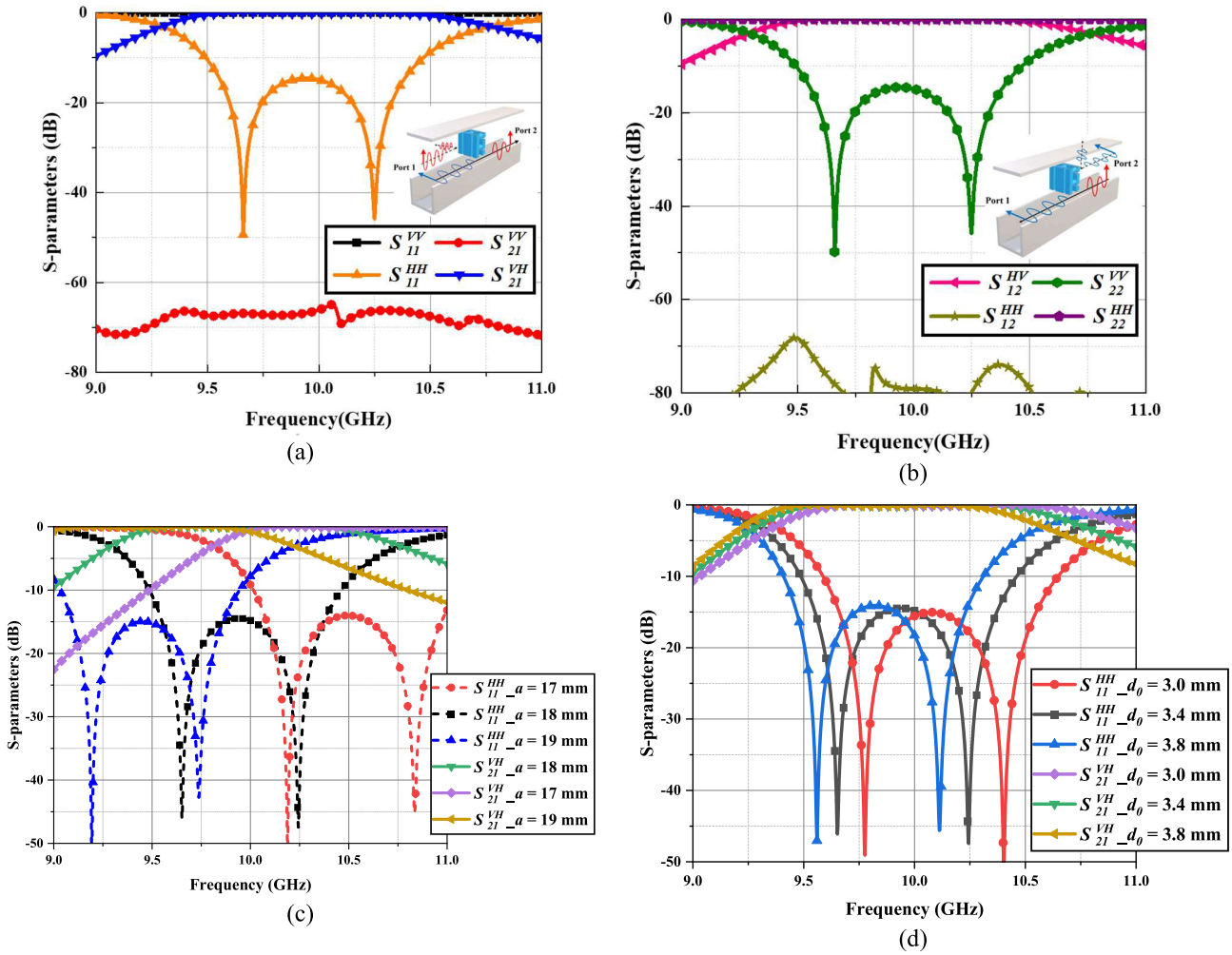

Fig. 5. Co- and cross-polarization S-parameters (a) from Ports 1 to 2 and (b) from Ports 2 to 1. The parameter sweeps for (c) side length $\boldsymbol{a}$ and (d) metal thickness $\boldsymbol{d_0}$.

The polarization conversions in the frequency range of 9.5–10.5 GHz exhibit low insertion loss, varying from 0.1 to 0.6 dB, as shown in Fig. 5(a). Simultaneously, the reflection coefficients of horizontally polarized waves are all above 10 dB, indicating high polarization conversion efficiency and good matching. On the other hand, the vertically polarized waves incident from Port 1 are entirely reflected, demonstrating a high degree of isolation. The transmission from Ports 2 to 1 shown in Fig. 5(b) is entirely symmetrical, with the only difference being the polarization reversal. As aforementioned, the structure can be regarded as a $\lambda/2$ slot resonator, where the slot length is close to half of the wavelength at the resonance frequency. The length $\boldsymbol{a}$ of the structure and the thickness $\boldsymbol{d_0}$ of the layers are two main parameters responsible for the resonance frequency, as shown in Fig. 5(c) and (d). Both parameters of the metamaterial influence its resonant frequency, with an increase in its physical dimensions causing the operational frequency to shift toward lower frequencies. This effect is similarly observed with variations in its thickness. Carefully selecting the values of parameters $\boldsymbol{a}$ and $\boldsymbol{d_0}$ can enable the Meta-OMT to operate within the desired frequency band.

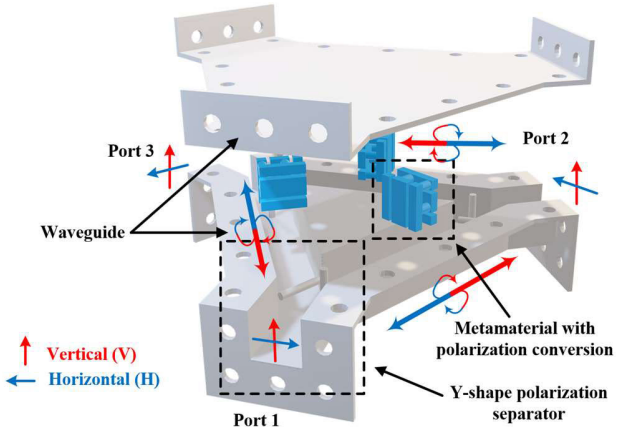

Fig. 6. Explosion diagram of the Meta-OMT structure, where the color-matched vertical and horizontal polarizations of the EM waves are converted when passing through the metamaterial pieces.

C. Meta-OMT Working Principle

The Meta-OMT structure, combining the Y-shaped polarization separator with metamaterial inclusion, is depicted in Fig. 6. It consists of three waveguide channels, each with a

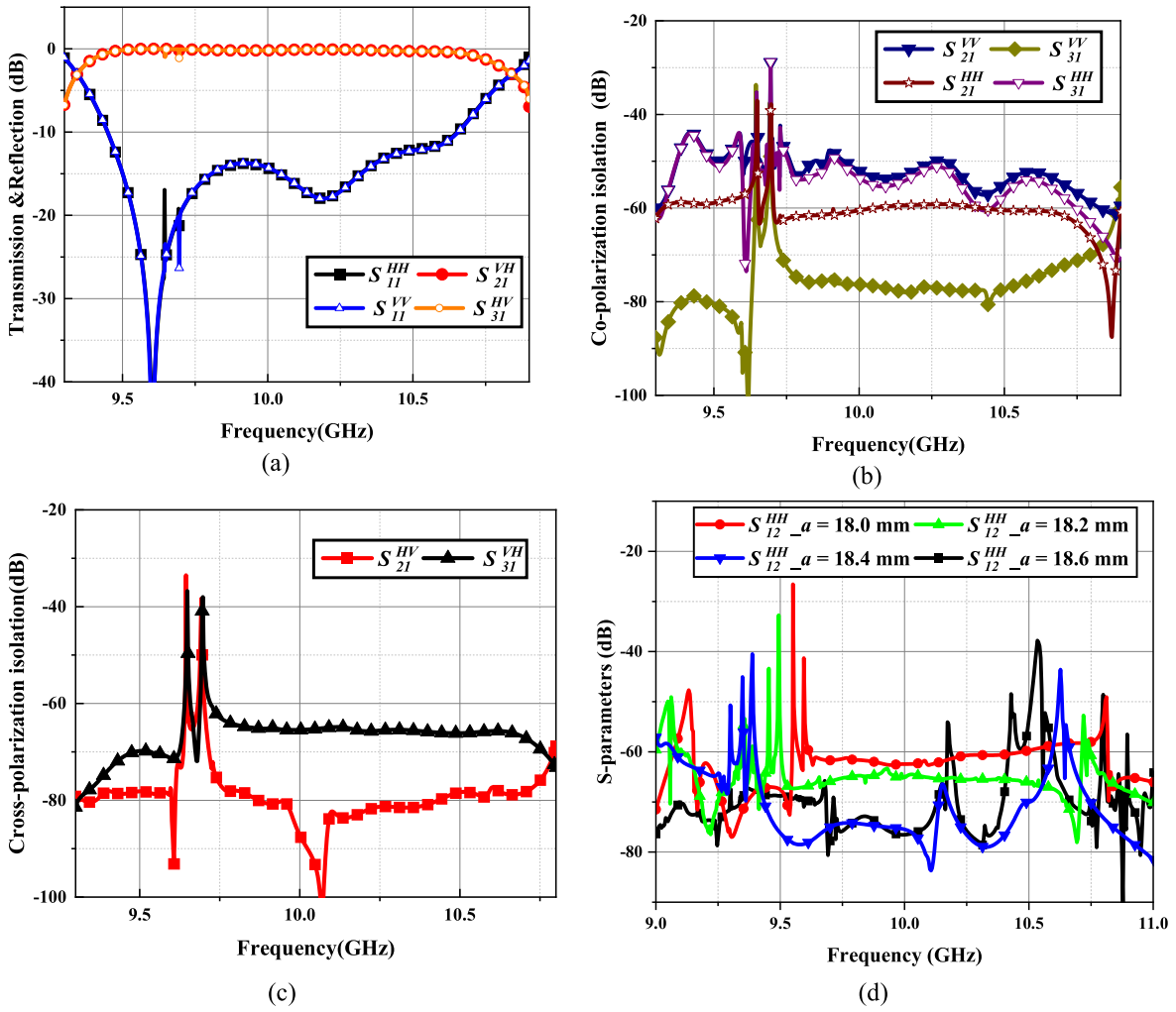

Fig. 7. Simulated S-parameters of Meta-OMT. (a) Transmission and reflection. (b) Co-polarization isolation. (c) Cross-polarization isolation. (d) S-parameter sweep of S_{12}^{HH} for the length $\boldsymbol{a}$ of the waveguide with a step of 0.2 mm.

length of 100 mm. Three pieces of metamaterial inserts enable polarization selection and rotation. They are placed in the middle of the waveguide channels, connected by the Y-shaped polarization separator.

The principle of the Meta-OMT operation is as follows. Let us assume Port 1 is an input port. When the signals are fed from Port 1, they can be represented by the superposition of the horizontally and vertically polarized EM waves at the bifurcation of the Y-shaped junction of the polarization separator. The vertically polarized signal travels to Port 3 and undergoes rotation by the metamaterial to become a horizontally polarized wave. Due to the presence of the Y-shaped polarization separator at Port 3, the rotated horizontally polarized wave can be transmitted only to the receiver at Port 3. On the other hand, the horizontally polarized signal input from Port 1 travels to Port 2 and undergoes polarization rotation by the metamaterial to become a vertically polarized signal at Port 2.

It is worth noting that the metamaterial itself also has polarization selection functionality. The advantage of separating the electromagnetic wave polarizations at the junction is twofold.

1) It reduces wave reflection, improves impedance matching, and achieves better coupling.
2) If orthogonal signals are not duly separated at the input, multipath effects can cause their interference. This interference can lead to signal enhancement or attenuation and causes the received signals to exhibit multiple components with different phases and amplitudes.

The presented characteristics of the Y-shaped polarization separator describe the overall performance of the Meta-OMT. Due to the structure symmetry, the port parameters are identical. Therefore, when analyzing the performance of the Meta-OMT, it is sufficient to consider only one input port. As shown in Fig. 7(a), the orthogonal signals from Port 1 are transmitted to Ports 2 and 3, respectively, with very high and consistent transmission coefficients. Within the operating frequency band of 9.4–10.6 GHz, the insertion loss varies from 0.1 to 0.5 dB, and the reflection coefficient ranges from 10 to 50 dB. Moreover, the co-polarization isolation between Port 1 and Ports 2 and 3 shown in Fig. 7(b) is above 40 dB in the operating frequency range, indicating a good isolation performance. As depicted in Fig. 7(c), the isolation between the vertically polarized signal at Port 1 and the horizontally polarized signal at Port 2 is also above 40 dB, demonstrating the same level of performance as the isolation between Ports 1 and 3. It is necessary to mention that the spikes, appearing

at ~9.6 GHz in the simulated S-parameter, represent resonances caused by the coupling between metamaterials and the metallic pins. The frequency and amplitude are largely affected by the radius $\boldsymbol{w_1}$ of pins and the distance $\boldsymbol{h_1}$ between pins and metamaterials. These resonances are quite small for co- and cross-polarization isolation with an amplitude below 40 dB and can be suppressed by increasing the size of the waveguide, which helps decrease the interference between the waves reflected from the metamaterial inserts and the propagating waves, but with a risk of new spikes at higher frequencies. As shown in Fig. 7(d), S_{12}^{HH} was chosen for parameter sweep for its stronger resonance compared with other S^{HH}-parameters. With the increasing length $\boldsymbol{a}$ of the waveguide, the spikes at 9.6 GHz shift to lower frequency and become weaker till disappear (the black line for $\boldsymbol{a} = 18.6$ mm). However, new spikes appear at higher frequencies and also shift to lower frequencies becoming stronger.

The Meta-OMT exhibits the three-port symmetry and enables all ports to serve as inputs of the orthogonal signals subjected to polarization separation and conversion. This expands the application range of the device beyond just OMT functionality. The design utilizes the polarization separation capability of the metamaterial, providing the Meta-OMT with isolation levels exceeding 40 dB for both co-polarization and cross-polarization signals. By leveraging the compactness and flexibility of the metamaterial structure, this OMT gives greater freedom for the device to become smaller and lighter and offers enhanced portability and versatility.

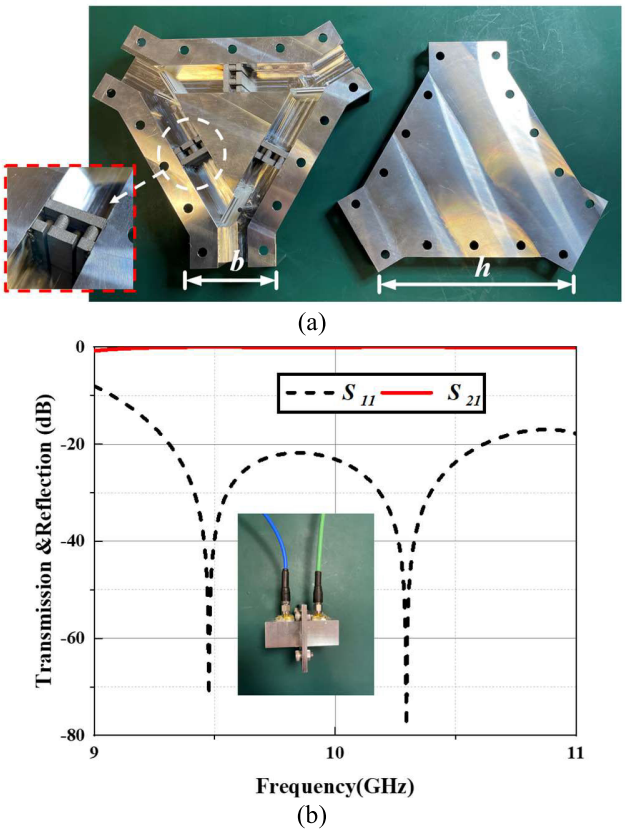

Fig. 8. (a) Prototype of the Meta-OMT with dimensions: $\boldsymbol{b} = 40$ mm and $\boldsymbol{h} = 130$ mm. (b) Measured transmission and reflection coefficients of the adapters.

III. Fabrication and Measurements

A. Mechanical Design and Testing Environments

The complex structure of the proposed device requires a thorough fabrication of its prototype. Therefore, we have adopted a combination of CNC machining and metal 3-D printing. The OMT waveguide structure produced by the CNC precision machining consists of two parts: the main body structure and the sealing cover shown in Fig. 8(a). They are tightly connected by screws at the perimeter. The metamaterial polarization rotator produced by 3-D metal printing is welded in the middle of the waveguide channel, and extra welding lines are polished to minimize their effect on the OMT performance. The device prototype is shown in Fig. 8(a). Since the waveguide ports of the designed OMT have a square cross section, the three adapters are specifically designed for testing the prototype. The input port of the adapter is a 3.5-mm SMA extended connector, and the adapter shown in the inset of Fig. 8(b) is machined using the same CNC process.

Due to the limitations of the adapter, which can only handle a single polarization of electromagnetic wave, the orientation of the SMA probe in the adapter needs to be changed manually for the desired polarization direction of the input–output wave during testing. Additionally, the vector network analyzer (VNA) used for testing has only two ports, allowing testing of S-parameters between two ports at a time. The remaining port is terminated into a 50-Ω matching load. The test setups for measuring the S-parameters of the cross-polarization ports are shown in Fig. 9. Taking input port 1 and output port 2 as an example, a horizontally polarized electromagnetic wave is fed to port 1. Referring to the diagram in Fig. 9(a), a signal propagates to port 2 and is converted into a vertically polarized wave along the path. Therefore, the adapter at port 2 is oriented vertically to receive the vertically polarized electromagnetic wave. When testing co-polarization S-parameters, it is sufficient to align the adapters connected to the input and output ports. When both input port 1 and output port 3 are horizontally polarized, as shown in Fig. 9(b), the co-polarization isolation coefficient of the horizontally polarized electromagnetic signals is tested between ports 1 and 3.

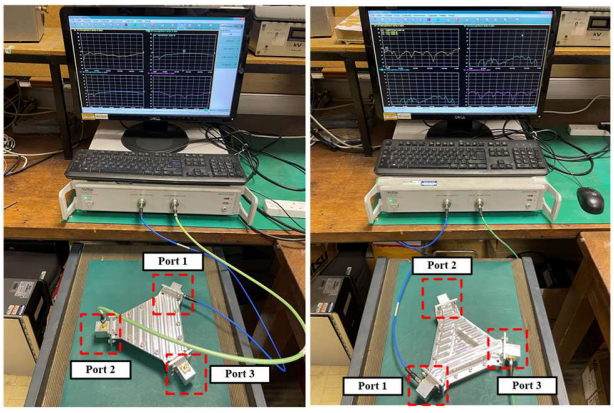

Fig. 9. Measurement setup for the Meta-OMT with an input at port 1 and outputs in ports 2 and 3. (a) Cross-polarization. (b) Co-polarization.

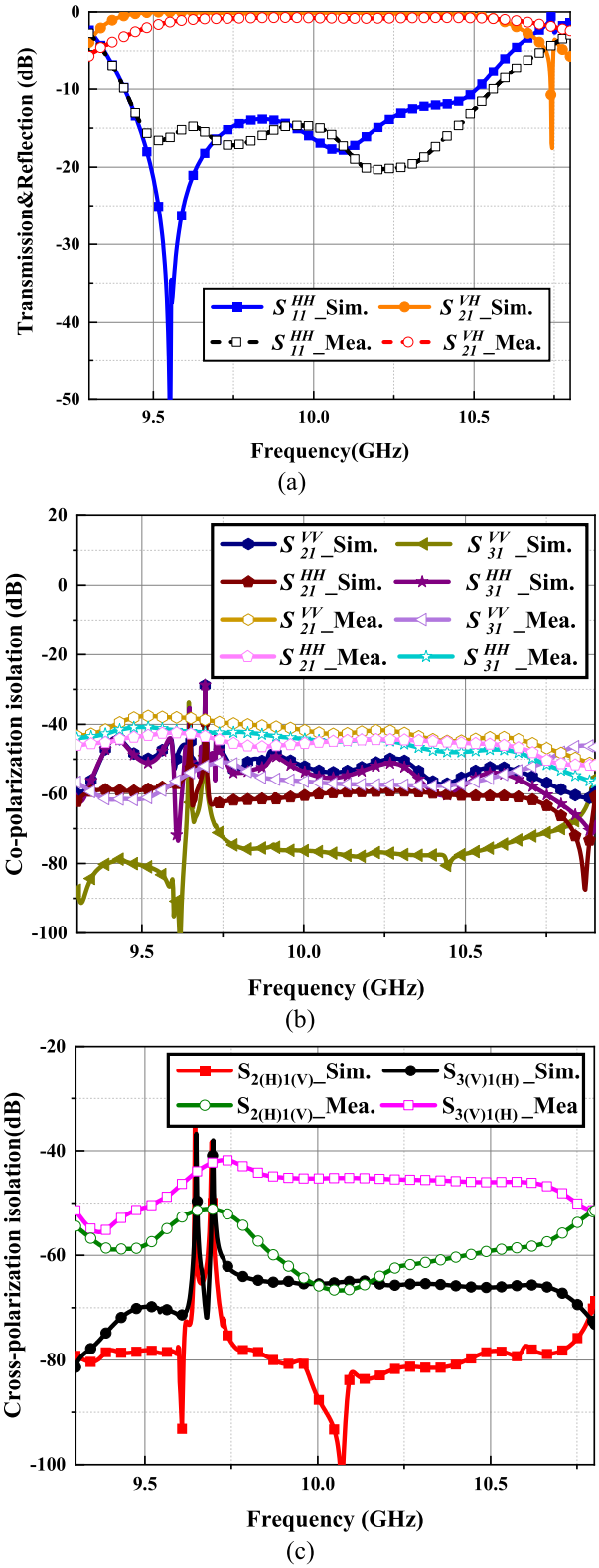

Fig. 10. Measured results of Meta-OMT. (a) Transmission and reflection. (b) Co-polarization isolation. (c) Cross-polarization isolation.

B. Measurement Results

The proposed Meta-OMT was made and then measured to validate its feasibility and evaluate its performance. The measurement results are shown in Fig. 10. The tested transmission coefficients exhibit slight frequency shifts toward higher frequencies, while good impedance matching and low insertion loss are obtained in the working frequency range. The co-polarization and cross-polarization isolation coefficients are shown in Fig. 10(b). The test results demonstrate excellent isolation performance. It is necessary to note that due to the fact that the simulated isolation already exceeded 50 dB in most of the frequency range, it is a challenging task to measure such small values accurately with the VNA.

The main sources of measurement uncertainties are related to fabrication inaccuracies.

1) The metamaterial inserts are fabricated using 3-D metal printing and then welded to the waveguide wall, so the protrusions caused by welding and the accuracy of the welding process affect the device's operational performance.
2) The contact between the metal pillars used for separating vertically polarized waves and the waveguide cover plate is not optimal. This leads to a small degradation of the achievable impedance matching.
3) Although a number of screws are used for sealing the upper cover plate, the contact between the top plate and the waveguide channel depends on the applied pressure. This leads to a small leakage, commensurate with the measured isolation.

Despite the intricacies of the design, prototype manufacturing, and testing of the proposed Meta-OMT, the test and simulation results demonstrate excellent device performance and feasibility of realizing the proposed Meta-OMT design.

The Meta-OMT described in this work is compared with asymmetric OMTs in Table I. The operational bandwidth of the Meta-OMT, being mostly limited by the metamaterials used, is comparable with that in [36] and [37]. However, the bandwidth can be effectively improved in several ways like the use of fractal geometries [38] or compact structures [39].

TABLE I
COMPARISON BETWEEN THE PROPOSED OMT WITH ASYMMETRIC OMTS

Ref.	[36]	[37]	This work
Frequency, GHz (Bandwidth)	7.2-8.2 (13%)	28-33 (16%)	**9.4-10.6 (12%)**
Isolation, dB	> 38	> 50	**> 40**
Return loss, dB	< -14.7	< -30	**< -10**
Insertion loss, dB	/	< 0.23	**< 0.5**
Size (λ_0^3)	/	4.1*7.1*1.9	**4.1*3.2*1.7**

IV. CONCLUSION

A novel OMT based on metamaterials with polarization conversion has been proposed in this article. By taking advantage of the compactness and flexibility of the metamaterial structure, this Meta-OMT provides more freedom of the device size, weight, and form factor. This work represents the first attempt to design OMTs primarily based on the concept of asymmetric metamaterials. The presented three-port Meta-OMT enables polarization separation and conversion for orthogonal

input signals from all three ports, thereby expanding its application beyond OMTs. The utilization of metamaterials' polarization separation capability enables the Meta-OMT to achieve over 40 dB of isolation for both co-polarization and cross-polarization signals. In addition, the Meta-OMT exhibits remarkably low insertion loss and high transmission within the operating frequency range of 9.4–10.6 GHz. The insertion loss varies from 0.1 to 0.5 dB, indicating minimal signal attenuation, while the consistently high transmission coefficients ensure efficient signal transmission. Leveraging the compactness and flexibility of the metamaterial structure, the OMT design offers increased flexibility in device size, resulting in a smaller and lighter form factor. This work presents the novel design of OMTs based primarily on asymmetric metamaterials, providing a fundamental design framework for future advancements in Meta-OMTs. These advancements have the potential to enable reconfigurable, tunable, and multifrequency band tuning capabilities for OMTs. Despite the challenges in Meta-OMT design, such as manufacturing complexity, frequency selectivity, and cost, the metamaterials still hold significant potential for widespread applications, playing a crucial role in innovative RF device designs. This work establishes a design framework for future improvements of OMTs using novel metamaterial structures. It enables reconfigurability, tuneability, and even the potential for enhanced tuning across multiple frequency bands.

ACKNOWLEDGMENT

The authors would like to acknowledge the help from colleagues at the High-Frequency Engineering Group, University of Liverpool, Liverpool, U.K.

REFERENCES

[1] S. J. Skinner and G. L. James, "Wide-band orthomode transducers," *IEEE Trans. Microw. Theory Techn.*, vol. 39, no. 2, pp. 294–300, Feb. 1991, doi: 10.1109/22.102973.

[2] R. D. Tompkins, "A broad-band dual-mode circular waveguide transducer," *IEEE Trans. Microw. Theory Techn.*, vol. MTT-4, no. 3, pp. 181–183, Jul. 1956.

[3] A. Navarrini and R. L. Plambeck, "A turnstile junction waveguide orthomode transducer," *IEEE Trans. Microw. Theory Techn.*, vol. 54, no. 1, pp. 272–277, Jan. 2006, doi: 10.1109/TMTT.2005.860505.

[4] A. Navarrini and R. L. Plambeck, "Orthomode transducers for millimeter wavelengths," in *Proc. URSI North Amer. Radio Sci. Meeting*, Jul. 2007, pp. 22–26.

[5] A. M. Boøifot, E. Lier, and T. Schaug-Pettersen, "Simple and broadband orthomode transducer," *IEE Proc. H Microw., Antennas Propag.*, vol. 137, no. 6, pp. 396–400, Dec. 1990.

[6] G. Pisano et al., "A broadband WR10 turnstile junction orthomode transducer," *IEEE Microw. Wireless Compon. Lett.*, vol. 17, no. 4, pp. 286–288, Apr. 2007, doi: 10.1109/lmwc.2007.892976.

[7] A. Navarrini and R. Nesti, "Symmetric reverse-coupling waveguide orthomode transducer for the 3-mm band," *IEEE Trans. Microw. Theory Techn.*, vol. 57, no. 1, pp. 80–88, Jan. 2009, doi: 10.1109/tmtt.2008.2008943.

[8] M. A. Abdelaal and A. A. Kishk, "Ka-band 3-D-printed wideband groove gap waveguide orthomode transducer," *IEEE Trans. Microw. Theory Techn.*, vol. 67, no. 8, pp. 3361–3369, Aug. 2019, doi: 10.1109/TMTT.2019.2919630.

[9] D. Henke and S. Claude, "Minimizing RF performance spikes in a cryogenic orthomode transducer (OMT)," *IEEE Trans. Microw. Theory Techn.*, vol. 62, no. 4, pp. 840–850, Apr. 2014, doi: 10.1109/TMTT.2014.2309551.

[10] C. A. Leal-Sevillano, K. B. Cooper, J. A. Ruiz-Cruz, J. R. Montejo-Garai, and J. M. Rebollar, "A 225 GHz circular polarization waveguide duplexer based on a septum orthomode transducer polarizer," *IEEE Trans. Terahertz Sci. Technol.*, vol. 3, no. 5, pp. 574–583, Sep. 2013, doi: 10.1109/TTHZ.2013.2264317.

[11] R. W. Jackson, "A planar orthomode transducer," *IEEE Microw. Wireless Compon. Lett.*, vol. 11, no. 12, pp. 483–485, Dec. 2001, doi: 10.1109/7260.974553.

[12] P. K. Grimes, O. G. King, G. Yassin, and M. E. Jones, "Compact broadband planar orthomode transducer," *Electron. Lett.*, vol. 43, no. 21, pp. 1146–1147, 2007.

[13] M. A. Morgan, J. R. Fisher, and T. A. Boyd, "Compact orthomode transducers using digital polarization synthesis," *IEEE Trans. Microw. Theory Techn.*, vol. 58, no. 12, pp. 3666–3676, Dec. 2010.

[14] Y. Tao and Z.-X. Shen, "Design of compact orthomode transducers," in *IEEE MTT-S Int. Microw. Symp. Dig.*, Dec. 2008, pp. 38–42.

[15] Y. Tao and Z. Shen, "Design of broadband planar orthomode transducers using substrate integrated waveguide," in *Proc. Asia–Pacific Microw. Conf.*, Dec. 2008, pp. 1–4.

[16] M. K. Mandal, K. Wu, and D. Deslandes, "A compact planar orthomode transducer," in *IEEE MTT-S Int. Microw. Symp. Dig.*, Jun. 2011, pp. 1–4.

[17] M. Esquius-Morote, M. Mattes, and J. R. Mosig, "Orthomode transducer and dual-polarized horn antenna in substrate integrated technology," *IEEE Trans. Antennas Propag.*, vol. 62, no. 10, pp. 4935–4944, Oct. 2014, doi: 10.1109/TAP.2014.2341697.

[18] L. Gerhardt, F. C. C. de Castro, C. Müller, and M. C. F. de Castro, "Compact symmetric opposed port orthomode transducer," *IEEE Microw. Wireless Compon. Lett.*, vol. 29, no. 7, pp. 471–473, Jul. 2019, doi: 10.1109/LMWC.2019.2917770.

[19] I. Goode and C. E. Saavedra, "3-D printed dually symmetric orthomode transducer and horn antenna at X-band," *IEEE Open J. Antennas Propag.*, vol. 4, pp. 383–391, 2023, doi: 10.1109/OJAP.2023.3264250.

[20] J. L. Cano, A. Tribak, R. Hoyland, A. Mediavilla, and E. Artal, "Full band waveguide turnstile junction orthomode transducer with phase matched outputs," *Int. J. RF Microw. Comput.-Aided Eng.*, vol. 20, no. 3, pp. 333–341, May 2010.

[21] H. Schlegel and W. D. Fowler, "The ortho-mode transducer offers a key to polarization diversity in EW systems," *Microw. Syst. News*, no. 9, pp. 65–70, Sep. 1984.

[22] I. J. Dilworth, "A microwave receiver and transmitter system for a propagation experiment'," in *Proc. Radio Receiv. Associated Syst.*, Jul. 1981, pp. 319–323.

[23] J. R. Brain, "The design and evaluation of a high performance 3 m antenna for satellite communication," *Marconi Rev.*, vol. 41, pp. 218–236, 4th Quart. 1978.

[24] C. A. Leal-Sevillano, Y. Tian, M. J. Lancaster, J. A. Ruiz-Cruz, J. R. Montejo-Garai, and J. M. Rebollar, "A micromachined dual-band orthomode transducer," *IEEE Trans. Microw. Theory Techn.*, vol. 62, no. 1, pp. 55–63, Jan. 2014, doi: 10.1109/TMTT.2013.2292611.

[25] J. M. Rebollar, J. Esteban, and J. De Frutos, "A dual frequency OMT in the Ku band for TT&C applications," in *Proc. IEEE Antennas Propag. Soc. Int. Symp., Dig. Antennas, Gateways Global Netw., USNC/URSI Nat. Radio Sci. Meeting*, Atlanta, GA, USA, Jun. 1998, pp. 2258–2261, doi: 10.1109/aps.1998.701748.

[26] J. M. Rebollar and J. de Frutos, "Dual-band compact square waveguide corrugated polarizer," in *Proc. IEEE Antennas Propag. Soc. Int. Symp., Dig. Antennas, Gateways Global Netw., USNC/URSI Nat. Radio Sci. Meeting*, Orlando, FL, USA, 1999, pp. 962–965, doi: 10.1109/aps.1999.789472.

[27] B. A. Munk, *Metamaterials: Critique and Alternatives*. Hoboken, NJ, USA: Wiley, 2009.

[28] C. L. Holloway, E. F. Kuester, J. A. Gordon, J. O'Hara, J. Booth, and D. R. Smith, "An overview of the theory and applications of metasurfaces: The two-dimensional equivalents of metamaterials," *IEEE Antennas Propag. Mag.*, vol. 54, no. 2, pp. 10–35, Apr. 2012, doi: 10.1109/MAP.2012.6230714.

[29] D. R. Smith, W. J. Padilla, D. C. Vier, S. C. Nemat-Nasser, and S. Schultz, "Composite medium with simultaneously negative permeability and permittivity," *Phys. Rev. Lett.*, vol. 84, no. 18, pp. 4184–4187, May 2000.

[30] J. Han and R. Chen, "Broadband metasurface for polarization conversion and asymmetric transmission at X-band," in *Proc. IEEE Int. Conf. Comput. Electromagn. (ICCEM)*, Singapore, Aug. 2020, pp. 232–233, doi: 10.1109/ICCEM47450.2020.9219339.

[31] M. I. Khan, B. Hu, Y. Chen, N. Ullah, M. J. I. Khan, and A. R. Khalid, "Multiband efficient asymmetric transmission with polarization conversion using chiral metasurface," *IEEE Antennas Wireless Propag. Lett.*, vol. 19, no. 7, pp. 1137–1141, Jul. 2020, doi: 10.1109/LAWP.2020.2991521.

[32] M. I. Khan, Q. Fraz, and F. A. Tahir, "Ultra-wideband cross polarization conversion metasurface insensitive to incidence angle," *J. Appl. Phys.*, vol. 121, no. 4, Jan. 2017, Art. no. 045103.

[33] J. Loncar, A. Grbic, and S. Hrabar, "A reflective polarization converting metasurface at *X*-band frequencies," *IEEE Trans. Antennas Propag.*, vol. 66, no. 6, pp. 3213–3218, Jun. 2018.

[34] M. I. Khan, Z. Khalid, and F. A. Tahir, "Linear and circular-polarization conversion in X-band using anisotropic metasurface," *Sci. Rep.*, vol. 9, no. 1, p. 4552, Mar. 2019.

[35] C. Caloz and A. Sihvola, "Electromagnetic chirality—Part 1: The microscopic perspective [electromagnetic perspectives]," *IEEE Antennas Propag. Mag.*, vol. 62, no. 1, pp. 58–71, Feb. 2020.

[36] H. Saeidi-Manesh, S. Saeedi, M. Mirmozafari, G. Zhang, and H. H. Sigmarsson, "Design and fabrication of orthogonal-mode transducer using 3-D printing technology," *IEEE Antennas Wireless Propag. Lett.*, vol. 17, no. 11, pp. 2013–2016, Nov. 2018, doi: 10.1109/LAWP.2018.2847654.

[37] G. Addamo et al., "Additive manufacturing of Ka-band dual-polarization waveguide components," *IEEE Trans. Microw. Theory Techn.*, vol. 66, no. 8, pp. 3589–3596, Aug. 2018, doi: 10.1109/TMTT.2018.2854187.

[38] S. Moeini, "Homogenization of fractal metasurface based on extension of Babinet–Booker's principle," *IEEE Antennas Wireless Propag. Lett.*, vol. 18, no. 5, pp. 1061–1065, May 2019, doi: 10.1109/LAWP.2019.2909134.

[39] X. Q. Lin, H. F. Ma, D. Bao, and T. J. Cui, "Design and analysis of super-wide bandpass filters using a novel compact meta-structure," *IEEE Trans. Microw. Theory Techn.*, vol. 55, no. 4, pp. 747–753, Apr. 2007, doi: 10.1109/TMTT.2007.892811.

Lingqi Kong received the M.E. degree in electromagnetic field and microwave technology from the Nanjing University of Aeronautics and Astronautics, Nanjing, China, in 2022. He is currently pursuing the Ph.D. degree in electronics and electronical engineering at the University of Liverpool, Liverpool, U.K.

His current research interests include metamaterials, metamaterial-based RF devices, nonreciprocal devices, and self-biased circulators.

Yi Huang (Fellow, IEEE) received the B.Sc. degree in physics in Wuhan, China, in 1984, the M.Sc. (Eng.) degree in microwave engineering in Nanjing, China, in 1987, and the D.Phil. degree in communications from the University of Oxford, Oxford, U.K., in 1994.

He has been conducting research in the areas of antennas, wireless communications, applied electromagnetics, radar, and EMC since 1987. More recently, he has focused on new materials for antennas, wireless energy harvesting, and power transfer. His experience includes three years spent with NRIET (China) as a Radar Engineer and various periods with the Universities of Birmingham, Oxford, and Essex in the U.K. as a member of research staff. He worked as a Research Fellow at British Telecom Laboratories, Ipswich, U.K., in 1994 and then joined the Department of Electrical Engineering and Electronics, University of Liverpool, Liverpool, U.K., as a Faculty in 1995, where he is currently a Full Professor of wireless engineering and the Head of High-Frequency Engineering Group. He has published over 500 refereed article in leading international journals and conference proceedings and authored four books, including Antennas: from Theory to Practice (John Wiley, 2008 and 2021). He has received many patents and research grants from research councils, government agencies, charities, the EU, and industry.

Dr. Huang was a recipient of over ten awards (e.g., BAE Systems Chairman's Award 2017, IET, and Best Paper Awards). He has served on a number of national and international technical committees and has been an Editor, an Associate Editor, or a Guest Editor of five international journals (including IEEE AWPL from 2016 to 2022). In addition, he has been a keynote/invited speaker and organizer of many conferences and workshops (e.g., IEEE iWAT2010, LAPC2012, and EuCAP2018/2024). He is at present the Editor-in-Chief of Wireless Engineering and Technology, the UK and Ireland Rep to the European Association of Antenna and Propagation (EurAAP), 2016 to 2020, 2022-date, a Fellow of IET, a Member, IEEE AP-S New Technology Directions Committee, and a Distinguished Lecturer of IEEE AP-S.

Alexander G. Schuchinsky (Fellow, IEEE) received the Ph.D. degree in radiophysics from Leningrad Electrotechnical University (USSR), Saint Petersburg, Russia, in 1983 and 1988, respectively, and holds the academic title of Senior Research Scientist.

From 1973 to 1994, he was with the Microwave Electromagnetics Laboratory, Rostov State University, Rostov-on-Don, Russia. From 1994 to 2002, he was a Chief Engineer with Deltec-Telesystems, Wellington, New Zealand. From 2002 to 2015, he was with Queen's University Belfast, Belfast, U.K. He is currently an Honorary Fellow with the University of Liverpool, Liverpool, U.K. He has authored three international patents, four book chapters, and over 250 refereed journal and conference papers. His current research interests include hexaferrites, self-biased nonreciprocal devices, and passive nonlinearities in microwave circuits.

Dr. Schuchinsky was the co-recipient of the IEEE 2010 Microwave Prize, and received the 2012 V.G. Sologub Award for contribution to Computational Electromagnetics. He was a co-founder and a General Co-Chair of the series of annual conferences "Metamaterials-International Congress on Advanced Electromagnetic Materials in Microwaves and Optics." He was a founding member of the European Virtual Institute for Artificial Electromagnetic Materials and Metamaterials, where he served on the Board of Directors. He was a co-founder and member of the Steering Committee of the European Doctoral Programs on Metamaterials. He was a member of the European Physical Society and a Fellow of the Higher Education Academy, U.K.